Mon. Not. R. Astron. Soc. **000**, 1–5 (2002) Printed 1 February 2008 (MN LATEX style file v2.2)

A long hard look at MCG–6-30-15 with *XMM-Newton*

A. C. Fabian,[1⋆], S. Vaughan,[1] K. Nandra,[2,3] K. Iwasawa,[1] D. R. Ballantyne,[1] J. C. Lee,[4] A. De Rosa,[1,5] A. Turner[1] and A. J. Young[6]
[1]*Institute of Astronomy, University of Cambridge, Madingley Road, Cambridge CB3 0HA*
[2]*Laboratory for High Energy Astrophysics, NASA/Goddard Space Flight Center, Greenbelt, MD 20771, USA*
[3]*Universities Space Research Association*
[4]*Massachusetts Institute of Technology, Center for Space Research, 77 Massachusetts Ave. NE80, Cambridge, MA 02139, USA*
[5]*IASF/CNR, Roma, Italy*
[6]*Astronomy Department, University of Maryland, College Park, MD 20742, USA*

arXiv:astro-ph/0206095v1 6 Jun 2002

Accepted 6/6/2002; submitted 30/5/2002; in original form 3/4/2002

ABSTRACT
We present first results from a 325 ks observation of the Seyfert 1 galaxy MCG–6-30-15 with *XMM-Newton* and *BeppoSAX*. The strong, broad, skewed iron line is clearly detected and is well characterised by a steep emissivity profile within $6r_{\rm g}$ (i.e. $6GM/c^2$) and a flatter profile beyond. The inner radius of the emission appears to lie at about $2r_{\rm g}$, consistent with results reported from both an earlier *XMM-Newton* observation of MCG–6-30-15 by Wilms et al. and part of an *ASCA* observation by Iwasawa et al. when the source was in a lower flux state. The radius and steep emissivity profile do depend however on an assumed incident power-law continuum and a lack of complex absorption above 2.5 keV. The blue wing of the line profile is indented, either by absorption at about 6.7 keV or by a hydrogenic iron emission line. The broad iron line flux does not follow the continuum variations in a simple manner.

Key words: galaxies: active – galaxies: Seyfert: general – galaxies: individual: MCG–6-30-15 – X-ray: galaxies

1 INTRODUCTION

The Seyfert 1 galaxy MCG–6-30-15 has played an important role in studies of accretion onto black holes due to the presence of a broad, skewed iron line in its X-ray spectrum (Tanaka et al. 1995). The shape of the line seen with *ASCA* is consistent with emission from the surface of an accretion disc extending from about 6 to more than 40 gravitational radii ($6-40r_{\rm g}; r_{\rm g}=GM/c^2$) inclined at about 30 deg to the line of sight (Fabian et al. 1995). Occasionally the red (i.e. lower energy) wing of the line is seen to extend below 4 keV (Iwasawa et al. 1996; 1999). This can be explained by the disc extending within $6r_{\rm g}$ which may imply the black hole must be rapidly spinning. The presence of the broad iron line in MCG–6-30-15 has been confirmed by *BeppoSAX* (Guainazzi et al. 1999), *XMM-Newton* (Wilms et al. 2001) and *Chandra* (Lee et al. 2002).

Here we present preliminary results from a long 325 ks observation of MCG–6-30-15 made with *XMM-Newton*. The source was at a similar flux level to the previous *ASCA* observations, and about 70 per cent brighter than during the earlier 100 ks *XMM-Newton* observation reported by Branduardi-Raymont et al. (2001) and Wilms et al. (2001). Simultaneous observations were made with *BeppoSAX*, providing coverage from $\sim$0.2–100 keV. The present work focuses on the spectrum above 2.5 keV and the iron-K line features; absorption and emission features below 2 keV due to oxygen and other elements will be discussed more fully in later work.

2 DATA REDUCTION

MCG–6-30-15 was observed by *XMM-Newton* (Jansen et al. 2001) over the period 2001 July 31 – 2001 August 5 (rev. 301, 302 and 303), during which all instruments were operating nominally. The present analysis is restricted to the data from the European Photon Imaging Cameras (EPIC). Both the EPIC MOS cameras (Turner et al. 2001) and the EPIC pn camera (Strüder et al. 2001) were operated in small window mode and used the medium filter. Extraction of science products from the Observation Data Files (ODFs) followed standard procedures using the *XMM-Newton* Science Analysis System v5.2 (SAS).

The EPIC data were processed using the standard SAS processing chains. Source data were extracted from circular regions of radius 30 arcsec from the processed MOS and pn images and background events were extracted from regions in the small window least effected by source photons. These showed the background to be relatively low and stable throughout the observation, with the exception of the final few ks of each revolution where the background rate increased. Data from these periods were ignored. The total amount of "good" exposure time selected was 315 ks and 227 ks

⋆ E-mail: acf@ast.cam.ac.uk

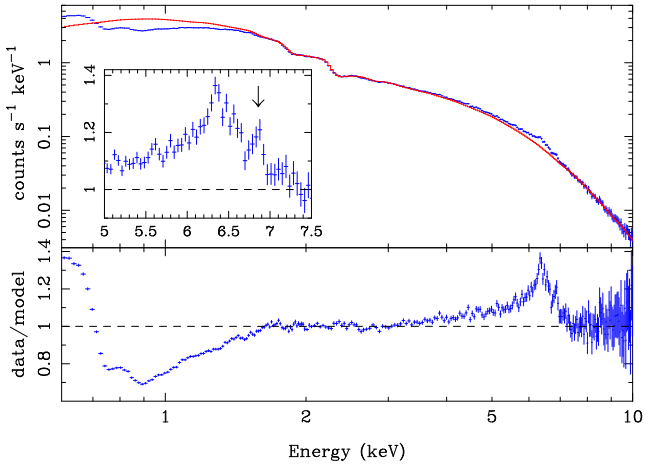

Figure 1. Combined MOS spectrum (the data were combined for plotting purposes only) and ratio of data to a power-law model joining the 2–3 keV data and 7.5–10 keV data. As this is not a realistic model for the continuum the residuals should be considered merely as representative of the spectral complexity. The inset panel shows a close-up of the iron line region with the 6.9 keV feature marked.

for MOS and pn, respectively. (The lower pn exposure is due to the lower "live time" of the pn camera in small-window mode, $\sim$71 per cent).

The ratios of event patterns as a function of energy showed there is negligible pile-up in the pn data but the MOS data suffer slightly from pile-up. A comparison of the data extracted including and excluding events from the central 10 arcsec of the source region showed only a slight flattening ($\Delta\Gamma \sim 0.06$) in the piled-up spectrum. This small effect was ignored in order to increase the number of source counts.

Events corresponding to patterns 0–12 (single–quadruple pixel) were extracted from the MOS cameras and patterns 0–4 (single+double) were used for the pn spectral analysis, after checking for consistency with the pattern 0 (single pixel event) data. The total number of photons extracted from the source region was 6.23×10^6 for the pn and 2.35×10^6 for each MOS camera. The *BeppoSAX* data were processed in the standard manner (Fiore et al. 1999).

3 SPECTRAL ANALYSIS

The spectral calibration of the EPIC cameras is still evolving. Using the publicly available software and response matrices, the remaining calibration-dependent residuals over the 2.5–10 keV range considered here should be at the $\lesssim 5$ per cent level (see Ferrando et al. 2002). However, there remain problems with the model for charge transfer inefficiency (CTI) for pn small-window mode data. In order to mitigate the effects of this, a conservative approach was used for the present analysis, with detailed spectral fitting results based on only the MOS data.

The source spectra were grouped such that each bin contains at least 20 counts and were fitted using XSPEC v11.1 (Arnaud 1996). The spectral responses used were `m1_medv9q19t5r5_all_15.rsp` for MOS1 (and similarly for MOS2) and `epn_sw20_sdY9_medium.rmf` for the pn. The quoted errors on the derived model parameters correspond to a 90 per cent confidence level for one interesting parameter (i.e. a $\Delta\chi^2 = 2.7$ criterion), unless otherwise stated, and fit parameters (specifically line and edge energies) are quoted for the rest frame of the source.

The EPIC MOS data show a spectral form remarkably similar to those seen in earlier *ASCA* observations, as illustrated in Fig 1 (cf. Fig. 1 of Iwasawa et al. 1996). The residuals around 6 keV have been interpreted as a broadened and redshifted iron Kα emission from a relativistic accretion disc (Tanaka et al. 1995). Only the *XMM-Newton* EPIC spectrum above 2.5 keV is examined here, to limit the effects of the complex soft X-ray absorption (see also Lee et al. 2001), a detailed treatment of which is beyond the scope of this Letter. This energy range also excluded the region around the detector Si K-edge (1.84 keV) and the mirror Au M-edge (2.3 keV). To better constrain the continuum, and in particular the Compton reflection component (e.g. George & Fabian 1991; Nandra & Pounds 1994), the *BeppoSAX* MECS and PDS data were also fitted simultaneously. The normalisations of the MOS and MECS data were allowed to vary independently, to account for differences in the absolute calibration, with the PDS normalisation tied to 0.86 times the MECS value (Fiore et al. 1999). Galactic absorption ($N_{\rm H} = 4.06\times10^{20}$ cm^{-2}; Dickey & Lockman 1990) was included in all the models discussed below.

3.1 Phenomenological model

The iron line residuals were initially parameterised using a simple model comprising a power law plus Compton reflection, narrow ($\sigma = 10$ eV) Gaussian at 6.4 keV and a broad Gaussian whose energy and width were free parameters. The Compton reflector was assumed to be a neutral, static slab subtending a solid angle of 2π sr at the X-ray source, inclined at $i = 30$ deg, and having solar elemental abundances (Magdziarz & Zdziarski 1995). The primary continuum was a power law with an exponential cutoff at a fixed energy of 400 keV (constraints on the reflection and continuum parameters are discussed later). This model gave a good overall fit with $\chi^2 = 984.1$ for 1034 degrees of freedom (dof). The broad line component had an energy $E = 4.8 \pm 0.3$ keV, a width of $\sigma = 1.8 \pm 0.2$ keV and equivalent width $EW = 527 \pm 70$ eV. The narrow, 6.4 keV "core" had $EW = 38 \pm 10$ eV and peaked very close to 6.4 keV, with $E = 6.40 \pm 0.04$ keV if allowed to be free.

Very narrow components to the iron line, unresolvable by EPIC, have been observed in the *Chandra* HETGS spectra of several Seyferts (Yaqoob et al. 2002). They may be identified with emission from, e.g. the BLR or molecular torus. Such narrow lines are not ubiquitous, however, and allowing the 6.4 keV component to have a finite width is resolved with a width corresponding to $FWHM \approx 30,000$ km s^{-1} and $EW = 120$ eV. The fit is excellent, the parameters are given in Table 1 (model 1). A preliminary analysis of the pn data gave generally consistent results and in particular the core of the line was again resolved. See also Lee et al. (2002). The large width of the line core suggests that this also arises in the disc, rather than at a greater distance (cf. NGC 5548; Yaqoob et al. 2001).

3.2 Relativistic line profiles

To provide a more physically realistic description of the data the line profile of Laor (1991) was used to describe a broad line from an accretion disc surrounding a rotating black hole. The disc was assumed to be in a low state of ionisation, with the rest energy of the line fixed at 6.4 keV. The fits were relatively insensitive to the outer radius of the disc, which was therefore fixed at $R_{\rm out} = 400r_{\rm g}$. The

Table 1. Results of simultaneous fits to the *XMM-Newton* MOS and *BeppoSAX* data. Line energies (E) and widths (σ) are given in units of keV and equivalent widths (EW) are given in eV. Disc radii (e.g. $R_{\rm in}$) are given in units of $r_{\rm g}$ and inclination (i) is given in degrees. The models are described in section 3.

model	Continuum		Broad Kα			Core Kα				χ^2/dof
	Γ	E	σ	EW	E	σ	EW			
1	1.93 ± 0.01	$4.29^{+0.09}_{-0.28}$	1.72 ± 0.09	383^{+25}_{-70}	6.40 ± 0.03	0.27 ± 0.06	119^{+9}_{-13}			888.2/1033
model	Continuum		Broad Kα							χ^2/dof
	Γ	i	$R_{\rm in}$	q	EW					
2	1.92 ± 0.01	38.3 ± 1.2	4.6 ± 0.4	$5.6^{+0.3}_{-0.6}$	308 ± 25					979.4/1034
model	Continuum			Broad Kα					6.9 keV line	χ^2/dof
	Γ	i	$R_{\rm in}$	$R_{\rm br}$	$q_{\rm in}$	$q_{\rm out}$	EW		EW	
3	1.96 ± 0.01	28.4 ± 1.0	2.0 ± 0.1	$6.2^{+3.4}_{-1.4}$	4.9 ± 0.6	2.6 ± 0.3	554 ± 56		29 ± 5	885.1/1031
4[1]	1.95 ± 0.04	27.8 ± 1.3	2.0 ± 0.2	$6.5^{+4.5}_{-1.4}$	4.8 ± 0.7	$2.5^{+0.2}_{-0.4}$	413^{+73}_{-89}		21 ± 5	856.2/1029

[1] This model includes $R_{\rm refl}$ and $E_{\rm fold}$ as free parameters, $A_{\rm Fe}=3$ and emission from Fe Kβ (see section 3.4).

free parameters in the model were: the inner radius of the disc, $R_{\rm in}$, the inclination, i, and the emissivity as a function of radius, which was parameterised as a power law of index q (i.e. R^{-q}). Both the line and the reflection spectrum were blurred using the kernel from the LAOR model. The fit parameters are given in Table 1 (model 2), the χ^2 is comparable to the broad plus narrow Gaussian model, but falls short of the best fitting χ^2 with two broad Gaussians (model 1). The reason for this is that, with a simple power law emissivity function, the Kerr line profile cannot simultaneously model the broad, red wing of the line and the narrower core around 6.4 keV. The preliminary pn analysis gave comparable results but suggested an even stronger red wing to the line.

3.3 Additional iron K components

Before exploring the red wing further it should be noted that there is some additional complexity in the line region at ~ 7 keV (see inset of Fig 1). Including an iron K-edge in model 2 provided a significant improvement in the fit ($\chi^2 = 908.2/1032$), with an edge energy of $E = 7.38\pm0.09$ keV and a depth of $\tau = 0.11\pm0.02$, similar to that discussed by Pounds & Reeves (2002). However, such an edge must have a physical origin; if it is due to neutral or near-neutral iron along the line of sight, then strong iron-L absorption is expected which is inconsistent with the soft X-ray spectrum (Lee et al. 2001). If the material is out of the line of sight and the edge is due to reflection off distant material, the reflection component must be very strong ($R\sim3$), which is then inconsistent with the relatively weak, narrow 6.4 keV iron line observed in the spectrum. Another possibility is that the edge arises from thick material partially covering the line of sight. This gives a comparable fit ($\chi^2 = 894.6/1032$) to the edge, with a covering fraction of ~ 0.16. Using this model the broad line parameters differed only slightly from those of model 2, and the broad, red wing of the line, extending within $6r_{\rm g}$, was still required in the fit.

Sako et al. (2002) suggested there may be significant absorption in the 6.4–6.7 keV range due to inner-shell transitions of ionised iron. This possibility was explored by including an absorption line in model 2. This gave a good fit ($\chi^2 = 923.9/1031\ dof$) with absorption line parameters $E = 6.74\pm0.05$ keV and $EW = 138\pm35$ eV. The relativistic line parameters differ only slightly, with the emissivity index changing to $q = 6.6\pm1.1$.

An alternative interpretation is that the complexity around 7.0 keV is in an emission component, identified with recombination emission by H-like iron. Adding a Gaussian to model 2 at

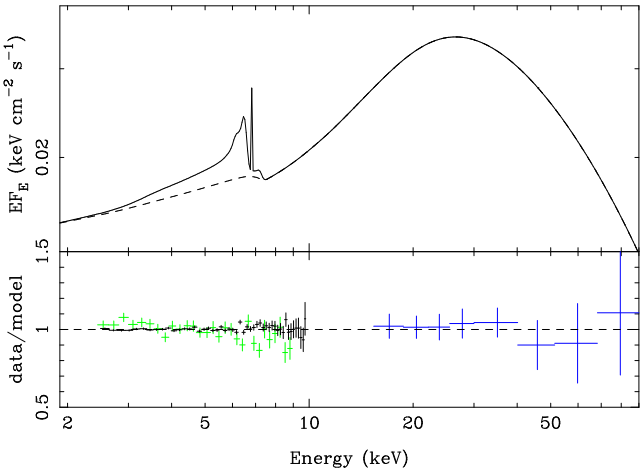

Figure 2. Model including relativistic iron line emission (model 4) and fit residuals for *XMM-Newton* MOS (black) and *BeppoSAX* MECS (green) and PDS (blue).

$E\approx6.9$ keV again improved the fit ($\chi^2 = 956.1/1032\ dof$) and gives best fitting parameters of $E = 6.91\pm0.03$ keV and $EW = 18\pm6$ eV. If a line of this strength is due to gas photoionised by the observed continuum then it must lie within a radius of $\sim 2\times10^{16}$ cm. Since it is not possible to unambiguously determine between absorption and emission as the source of complexity above 6.5 keV, both are considered in the following subsections.

3.4 More complex models

A steep emissivity function was required to model the red wing of the line (see also Wilms et al. 2001), but this gave too little flux from the outer parts of the disc to model the core of the line. This raises the possibility that the emissivity function is not a simple power-law. This was explored by using a broken power-law for the emissivity function, with emissivity index $q_{\rm in}$ from $R_{\rm in}$ to $R_{\rm br}$ and index $q_{\rm out}$ from $R_{\rm br}$ to $R_{\rm out}$. The fit parameters for this model are given in Table 1 (model 3).

This fit is not physically self-consistent for at least two reasons. Firstly it ignores the emission from Fe Kβ, which is expected at 7.05 keV. Secondly, the high EW of the line is not consistent with our assumptions about the reflection component, namely that it has $R_{\rm refl} = 1$, $i = 30$ deg, solar abundances and is neutral. In

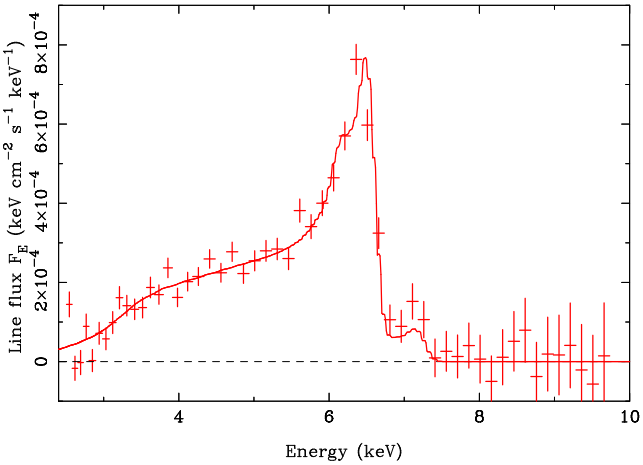

Figure 3. Relativistic iron line profile, shown in (F_ν) flux units, obtained from the ratio of the MOS data to best-fitting underlying continuum model (model 4), multiplied by the continuum model in flux units (as opposed to an "unfolded" plot). The crosses mark the data points and the solid line marks the line model.

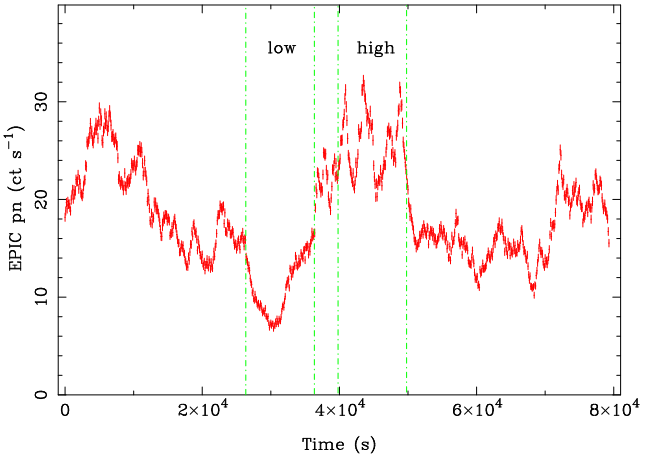

Figure 4. EPIC pn light curve (0.2–10 keV) for revolution 301 showing the intervals of low and high flux discussed in section 4.

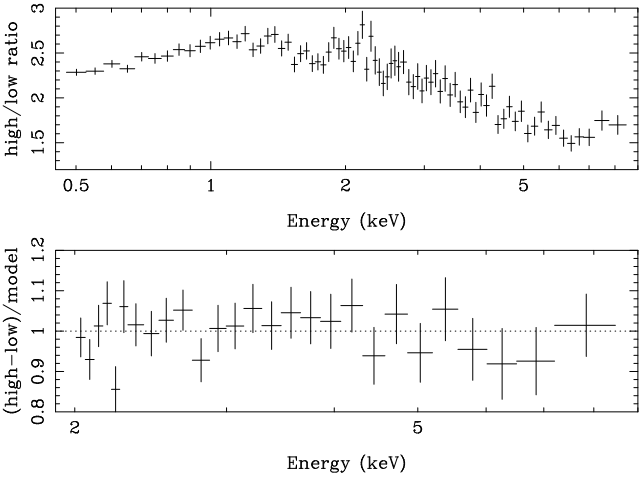

Figure 5. Comparison of the high-flux and low-flux pn spectra extracted from intervals marked on Fig. 4. Top panel: ratio of high-flux to low-flux spectrum. Bottom panel: comparison of the difference spectrum (high–low) to a power-law model.

such circumstances, considering the observed value of Γ, the predicted EW is only 140 eV (George & Fabian 1991). Two plausible possibilities are that the iron abundance in the accretion disc is higher than the solar value (see e.g. Lee et al. 1999), or that the reflection component is enhanced for some reason, for example due to anisotropy (Ghisellini et al. 1991) or geometry (Fabian et al. 2002).

The high abundance case was examined by fixing the iron abundance of the reflector to 3×solar in model 3. This in fact improved the overall fit compared to the solar abundance case ($\chi^2 = 877.2/1031\ dof$). Changes in the disc line parameters were negligible. The value of the cutoff energy can affect both the high energy spectral shape and the apparent strength of the reflection component. Allowing $E_{\rm cut}$ to be free in this fit gave $E_{\rm cut} = 241^{+228}_{-86}$ keV ($\chi^2 = 875.4/1030\ dof$). Allowing $R_{\rm refl}$ to be a free parameter further improved the fit, therefore this was also left free in model 4.

Model 4 comprised a power-law plus cold reflection (with overabundant iron, $A_{\rm Fe} = 3$), emission from iron Kα (6.40 keV) and Kβ (7.05 keV). The reflection plus line spectrum was then blurred using the LAOR kernel (with a broken power-law emissivity function). A narrow emission line at $E = 6.9$ keV (fixed) was also included in the model. This provided the best fitting model, with a cut-off energy $E_{\rm cut} = 122^{+90}_{-18}$ keV and $R_{\rm refl} = 2.2^{+1.1}_{-0.7}$, the other parameters are given in Table 1. The model and fit residuals are shown in Fig. 2 and the "fluxed" line profile based on this fit is shown in Fig. 3.

Including an absorption line instead of a 6.9 keV emission line gave a slightly poorer fit ($\chi^2 = 863.0/1027\ dof$) with line parameters $E = 6.74 \pm 0.02$ keV, $EW = 31 \pm 9$ eV (consistent with the prediction of Sako et al. 2002), and slight changes to the relativistic line parameters (in particular $R_{\rm br} = 3.9 \pm 0.7 r_{\rm g}$).

4 SPECTRAL VARIABILITY

As a first test for spectral variability around the iron line region pn spectra were extracted from 10 ks intervals around the minimum and maximum flux periods during revolution 301 (see Fig. 4). The average continuum fluxes during these intervals differ by $> \times 2$. The ratio of the two spectra is shown in the top panel of Fig. 5 and shows clear signs of spectral variability. There is a slight depression around 6.4 keV, indicating the iron line core is stronger (compared to the continuum) in the low-flux spectrum. The bottom panel of Fig. 5 shows the residuals from fitting a power-law model to the difference spectrum (i.e. high-flux minus low-flux spectrum). The difference spectrum is consistent with a power-law in the range 2-10 keV and indicates the iron line flux changed little between the two intervals. A detailed analysis of the spectral variability properties will be given in a forthcoming paper but these first results are consistent with the simple two component continuum model described in Shih et al. (2002).

The suggestion that the iron line was not as variable as the continuum was borne out by an examination of the RMS spectrum. Figure 6 shows the normalised RMS variability spectrum derived from the revolution 302 pn data. The RMS spectrum clearly shows that the fractional variability amplitude is suppressed at energies close to the iron line, compared to surrounding continuum bands (see also Inoue & Matsumoto 2001).

A further point to note is that the RMS spectrum (and the ratio

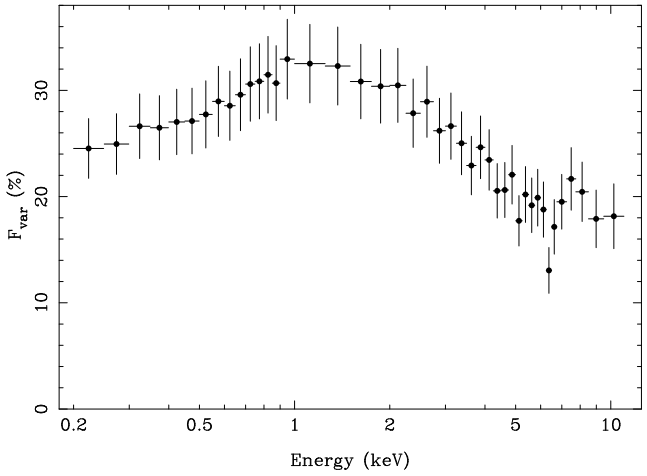

Figure 6. The RMS spectrum based on rev. 302 EPIC pn data. The errors are calculated as in Edelson et al. (2002) and should be considered conservative estimates of the true uncertainty.

of high/low spectra) are smooth in the 0.2–1.0 keV range. In particular, the absence of any feature at 0.7 keV in the spectral ratio is expected if the large drop at that energy (Fig 1) is due to absorption (with constant optical depth). For the drop to be the blue wing of an emission line (Branduardi-Raymont et al. 2001), the line intensity must be responding linearly to the continuum flux (unlike the iron line). An examination of the RGS spectra confirms this result.

5 DISCUSSION

A long observation with *XMM-Newton* and *BeppoSAX* of MCG–6-30-15 in its typical state has again confirmed the presence of the broad, skewed iron line. All the models considered above are formally acceptable ($\chi^2_\nu < 1.0$), and all include emission within $6r_{\rm g}$, consistent with emission from a disc around a spinning black hole.

Model 4 provides the best (in a χ^2-sense) and most physically self-consistent explanation of the data. In this model, the disc emissivity is described by a broken power-law in radius, and it is interesting to note that the break radius occurs at $\sim 6r_{\rm g}$. Beyond this radius the disc has an emissivity profile $q_{\rm out} \sim 2.5$ and produces an iron line with an equivalent width ~ 200 eV (the $5.5-6.5$ keV core of the line shown in Fig. 3), both close to the values expected from standard accretion disc models. Within $6r_{\rm g}$ the emissivity steepens, producing the strong low-energy tail to the line emission, also with an equivalent width ~ 200 eV, suggesting additional physics within this region beyond that expected from standard accretion disc models (see Wilms et al. 2001). The strong iron line is consistent with an enhanced reflection spectrum and an overabundance of iron or ionisation of the disc surface. This last possibility will be examined in a later paper.

The iron line parameters do, however, depend slightly on the assumptions made about the complex absorption. In particular all the above models formally assume the effects of ionised absorption are negligible above 2.5 keV, which is correct for absorption due to low-Z elements (e.g. O) but may not be true if there is absorption by higher-Z elements (e.g. Si, S). A preliminary analysis allowing for the possibility of Si and S edges did not change the requirement for a strong red wing to the iron line. A detailed analysis of the RGS data will yield constraints on the warm absorption (particularly on the low Z elements) and help remove existing degeneracies.

Future work to determine the spin must include emission from the immediate plunge region inside the innermost stable orbit (Reynolds & Begelman 1997; Agol & Krolik 2000) as well as returning radiation (Martocchia, Matt & Karas 2002).

ACKNOWLEDGEMENTS

Based on observations obtained with *XMM-Newton*, an ESA science mission with instruments and contributions directly funded by ESA Member States and the USA (NASA). ACF thanks the Royal Society for support.

REFERENCES

Agol E., Krolik J.H., 2000, ApJ, 528, 161
Arnaud, K. 1996, in: *Astronomical Data Analysis Software and Systems*, Jacoby, G., Barnes, J., eds., ASP Conf. Series Vol. 101, p17
Branduardi-Raymont, G., Sako, M., Kahn, S. M., Brinkman, A. C., Kaastra, J. S., Page, M. J., 2001, A&A, 365, L140
Dickey J. M., Lockman F. J. 1990, ARA&A 28, 215
Edelson, R. et al. 2002, ApJ, 568, 610
Fabian, A. C., Nandra, K., Reynolds, C. S., Brandt, W. N., Otani, C., Tanaka, Y., Inoue, H., Iwasawa, K. 1995, MNRAS, 277, L11
Fabian, A. C., Ballantyne, D. R., Merloni, A., Vaughan, S., Iwasawa, K., Boller, Th., 2002, MNRAS, 331, L35
Ferrando, P., et al. 2002, in *"New Visions of the X-ray Universe in the XMM-Newton and Chandra era"*, (astro-ph/0202372)
Fiore. F., Guainazzi, M., Grandi, P., 1999, Cookbook for *BeppoSAX* NFI Spectral Analysis
George, I. M., Fabian. A. 1991, MNRAS, 249, 352
Ghisellini, G., George, I. M., Fabian, A. C., Done, C., 1991, MNRAS, 248, 14
Guainazzi, M., et al. 1999, A&A, 341, L27
Inoue, H., Matsumoto, C., 2001, AdSpR, 28, 445
Iwasawa, K., et al. 1996, MNRAS, 282, 1038
Iwasawa, K., Fabian, A. C., Young, A. J., Inoue, H., Matsumoto, C., 1999, MNRAS, 306, L19
Jansen, F. et al. 2001, A&A, 365, L1
Laor, A., 1991, ApJ, 376, 90
Lee, J. C., Fabian, A. C., Brandt, W. N., Reynolds, C. S., Iwasawa, K., 1999, MNRAS, 310, 973
Lee, J. C., Fabian, A. C., Reynolds, C. S., Brandt, W. N., Iwasawa, K., 2000, MNRAS, 318, 857
Lee, J. C., Ogle, P. M., Canizares, C. R., Marshall, H. L.; Schulz, N. S., Morales, R., Fabian, A. C., Iwasawa, K., 2001, ApJ, 554, L13
Lee, J. C., et al. 2002, ApJ, 570, L47
Magdziarz, P., Zdziarski, A. A., 1995, MNRAS, 273, 837
Martocchia, A., Matt, G., Karas, V., 2002, A&A, 383, L23
Nandra, K., Pounds, K. A. 1994, MNRAS, 268, 405
Pounds, K. A., Reeves, J. N., 2002, in *New Visions of the X-ray Universe in the XMM-Newton and Chandra Era* (astro-ph/0201436)
Reynolds C.S., Begelman M.C., 1997, ApJ, 488, 109
Sako, M., et al. 2002, ApJ, submitted (astro-ph/0112436)
Shih, D. C., Iwasawa, K., Fabian, A. C., 2002, MNRAS, in press (astro-ph/0202432)
Strüder, L. et al. 2001, A&A, 365, L18
Tanaka, Y., et al. 1995, Nature, 375, 659
Turner, M. J. L. et al. 2001, A&A, 365, L27
Wilms, J., Reynolds, C. S., Begelman, M. C., Reeves, J., Molendi, S., Staubert, R., Kendziorra, E., 2001, MNRAS, 328, L27
Yaqoob, T., George, I. M., Nandra, K., Turner, T. J., Serlemitsos, P. J., Mushotzky, R. F., 2001, ApJ, 546, 759
Yaqoob, T., Goerge, I. M., Turner, T. J. 2002, in *"High Energy Universe at Sharp Focus: Chandra Science"*, eds. S. Vrtilek., E. M. Schlegel, L. Kuhi, (astro-ph/0111428)